Oxidation-induced degradation and performance fluctuation of solid oxide fuel cell Ni Anodes under simulated high fuel utilization conditions

Tatsuya Kawasaki,[a] Junko Matsuda,[b,f] Yuya Tachikawa,[a,b,d] Stephen Matthew Lyth,[c,e] Yusuke Shiratori,[a,b,d,f] Shunsuke Taniguchi,[b,d,f*] and Kazunari Sasaki[a-f]

Kyushu University

[a] Faculty of Engineering (Hydrogen Energy Systems),

[b] Center for Co-Evolutional Social Systems,

[c] International Institute for Carbon-Neutral Energy Research (WPI-I2CNER),

[d] Next-Generation Fuel Cell Research Center (NEXT-FC),

[e] Platform of Inter/Transdisciplinary Energy Research (Q-PIT)

[f] International Research Center for Hydrogen Energy,

744 Motooka, Nishi-ku, Fukuoka 819-0395, Japan

* Corresponding author

Prof. Dr. Shunsuke Taniguchi

Kyushu University, International Research Center for Hydrogen Energy

744 Motooka, Nishi-ku, Fukuoka 819-0395, Japan

(Tel) +81-92-802-6777, (Fax) +81-92-802-3223,

(Email) taniguchi.shunsuke.330@m.kyushu-u.ac.jp

Abstract

High fuel utilization (Uf) conditions in a small-scale electrolyte-supported solid oxide fuel cell (SOFC) with an Ni-ScSZ anode were approximated by adjusting the gas composition to correspond to that in the downstream region of an SOFC stack. At Uf = 80%, and with a cell voltage of 0.5 V, the ohmic resistance fluctuated slightly from the early stages of operation, and became much more significant after 80 h. High current density and large polarization were found to promote Ni agglomeration, leading to insufficient connectivity of the Ni nano-particles. At Uf = 95%, and with a cell voltage of 0.6 V, fluctuations in the polarization were observed at a much earlier stage, which are attributed to the highly humidified fuel. In particular, significant degradation was observed when the compensated anode potential (which incorporates the anode ohmic losses) approached the Ni oxidation potential. Ohmic losses in the anode are considered to influence Ni oxidation by exposing Ni near the electrolyte to a more oxidizing atmosphere with the increase in oxygen ion transport. Stable operation is therefore possible under conditions in which the compensated anode potential does not approach the Ni oxidation potential, assuming a stable interconnected Ni network.

Keywords

Fuel cell, Solid oxide, Anode, Nickel, Degradation

Introduction

Fuel cells can convert chemical energy into electricity with much higher efficiency than conventional internal combustion engines. They can utilize fossil fuels such as natural gas, biofuels, or hydrogen (produced either from renewable energy or fossil fuels). Increasing worldwide interest in sustainability, as symbolized by the Paris Agreement, has raised the expectations for fuel cells. Among the various types of fuel cells, solid oxide fuel cells (SOFCs) have several advantages, including fuel flexibility and high efficiency. Commercialization of SOFC systems has already started with residential and industrial applications, and demonstrations for a wider range of uses have been carried out. Moreover, their application to automobiles as a range extender for electromobility is attracting increasing interest.

For the widespread application and commercialization of SOFC systems, further improvements are required both in efficiency and durability. To raise the efficiency, the SOFC stack must utilize a much higher percentage of fuel for generating electricity. In conventional SOFC technology, the fuel utilization is limited to around 80% to avoid damaging the anode material, and the residual fuel is often combusted outside of the SOFC stack. Ni is a widely used anode material because of its combination of high electrochemical activity and steam reforming activity. However, when the stack is operated at fuel utilization higher than the upper limit, the Ni anode in the downstream region of the stack may be exposed to harsh conditions, such as high humidity and high oxygen partial pressure [1].

It has been reported that high humidity can accelerate Ni agglomeration in SOFC anodes [2], decreasing the triple-phase boundary (TPB) length, and thus leading to performance degradation. In some cases, this causes severe damage to the anode by disrupting the connectivity of the Ni network, impeding the electronic conduction [3,4]. There are several theories about the mechanism for anode degradation. One is that NiO_x (s) formed on the surface may enhance Ni-ion migration outward [5]. Another is that Ni_2-OH species formed at the surface cause Ni sintering by enhancing surface transport [6]. Another is that $Ni(OH)_2$ (g) may be the cause of Ni agglomeration because it has the highest vapor pressure, and a decrease in the amount of Ni has been reported to support this [2,7].

When the fuel concentration in the SOFC anode gets too low, Ni can be oxidized by the associated increase in oxygen partial pressure. Ni oxidation is generally accompanied by a change in morphology [8-10], which causes added performance degradation even after oxi-

dized Ni is reduced back to its metallic state. In the extreme case, volume expansion of Ni during oxidation can cause cracking of the anode or electrolyte, leading to severe degradation or even failure of the cell. Oxidation-reduction cycling also accelerates Ni agglomeration [8,10-13]. Ni can be oxidized electrochemically by the oxygen ions coming through the electrolyte [14-16]. Electrochemical oxidation is more likely to occur near the electrode reaction sites when a high current density is drawn from the cell without sufficient fuel supply.

The degradation phenomena of Ni anodes in SOFCs under extreme conditions are predictable. However, the upper limit of fuel utilization in practical use is not yet clear, especially under high current load. This study investigates the threshold conditions under which the Ni anode can maintain its performance as the fuel utilization and current density are increased, using both experimental and theoretical methods. A small-scale electrolyte-supported SOFC is used, and high fuel utilization up to Uf = 95% is simulated by adjusting the anode gas composition to approximate that downstream of an SOFC stack. High current density is applied by setting the cell voltage at 0.5 V or 0.6 V. Trigger factors leading to fatal degradation, the influence of anode potential on degradation, and fluctuation phenomena related to degradation are analyzed in detail.

Thermochemical equilibrium calculation

Figure 1 shows the phase stability diagram of the Ni-O-H system calculated by using thermochemical equilibrium calculation software (HSC Chemistry Ver. 9). The hydrogen partial pressure (pH_2) and the oxygen partial pressure (pO_2) resulting from the gas composition (100-x)% H_2 : x% H_2O (where x = 3 to 95%) are also plotted in red. Figure 1 (b) is an enlargement of the region highlighted in red. As the humidity (i.e. the water vapor pressure, pH_2O) increases, the pO_2 approaches the region where NiO is the most stable phase. The threshold pO_2 at the Ni/NiO phase boundary pO_2*, can be derived by the following equation:

$$pO_2^* = 1 / K_{Ni}$$

where K_{Ni} is the equilibrium constant of the reaction 2Ni (s) + O_2 (g) = 2NiO (s). This value is is $pO_2^* = 1.45\times10^{-14}$ bar ($\log pO_2^* = -13.84$) at 800°C, corresponding to an anode potential of 0.701 V versus atmospheric air (pO_2 = 0.21 bar). Even under highly humidified conditions

(5%H_2:95%H_2O), the pO_2 remains in the region where metallic Ni is most stable. However, when a current load is applied, the chemical potential of oxygen at the anode reaction sites (i.e. the solid anode surface) will increase, and the corresponding pO_2 may exceed the threshold pO_2* and enter the NiO phase. In general, the anode overpotential η is considered to be the increase in the chemical potential of oxygen at the anode reaction site, and the corresponding pO_2' increases according to the following equation [17]:

$$pO_2' = pO_2 \exp(4\eta F / RT)$$

where pO_2 is the environmental oxygen partial pressure; T is the temperature (K); F is the Faraday constant (C/mol); R is the gas constant (J $\cdot mol^{-1} \cdot K^{-1}$); and the anode overpotential η includes all of the factors (i.e. activation overpotential, concentration overpotential, etc.) that can increase the chemical potential of oxygen at the anode reaction sites. Therefore, the threshold pO_2 for the fuel gas fed to the anode will be affected by η and decrease to:

$$pO_2 = (1 / K_{Ni}) \exp(-4\eta F / RT).$$

Since pO_2 in the H_2:H_2O system is derived by the following equation:

$$pO_2 = pH_2O^2 / (pH_2^2 K_H)$$

where K_H is the equilibrium constant of the reaction $2H_2$ (g) + O_2 (g) = $2H_2O$ (g), the maximum allowable pH_2O determined by the Ni/NiO phase boundary, corresponding to the maximum fuel utilization in the H_2:H_2O system, is theoretically calculated by the following equation:

$$pH_2O_{max}\,(\%) = 100 / [1 + (K_{Ni} / K_H)^{1/2} \exp(2\eta F / RT)]$$

Figure 2 shows the maximum pH_2O calculated by the above equation for temperatures of 800°C, 900°C, and 1000°C. The maximum pH_2O changes slightly with temperature due to the temperature dependence of the Ni/NiO phase boundary. When the anode overpotential is less than 0.1 V, a pH_2O higher than 95% is permissible. When the anode overpotential is higher than 0.2 V, the pH_2O should be lower than 70% at 800°C. This provides theoretical limits to the fuel utilization in an SOFC.

The experimental results described below reveal that the anode overpotential should be evaluated by including ohmic losses in the anode as well as polarization (i.e. non-ohmic losses such as the activation overpotential and the concentration overpotential) because this also affects Ni oxidation. In a real SOFC system, it should be considered that the distribution of gas in the stack including possible gas leakage may reduce the upper limit of fuel utilization.

Experiments

Electrolyte plates made of ScSZ (10 mol% Sc_2O_3, 1 mol% CeO_2, 89 mol% ZrO_2, Daiichi Kigenso Kagaku Kogyo Co., Ltd.) with a thickness of 0.2 mm and diameter of 20 mm were used in this study. For the anode material, a mixture of 56 wt% NiO (Kanto Chemical Co., Inc.) and 44 wt% ScSZ was used for the anode functional layer, and a mixture of 80 wt% NiO and 20 wt% ScSZ was used for the anode current collecting layer. These mixtures were printed onto the electrolyte plates and sintered at 1300°C for 3 h. The thickness of the anode was approx. 50 to 60 μm. A mixture of 50 wt% LSM ($(La_{0.8}Sr_{0.2})_{0.98}MnO_3$, Praxair, Inc.) and 50 wt% ScSZ was used for the cathode. The cathode layers were sintered at 1200°C for 5 h. The electrode area was 8×8 mm (0.64 cm^2) and Pt mesh (80 mesh) was used as the current collector. A reference electrode made from Pt paste (U-3401, Metalor Technologies (Japan) Corp.) was attached to the cathode side to measure the anode and cathode potentials. The configuration of the cell is shown in Fig. 3. The distance between the edge of the cathode and the reference electrode was approx. 1.5 mm, which allowed us to detect potentials within the electrolyte with a thickness of 0.2 mm, based on a sufficiently small misalignment between the anode and cathode [18-19].

The cell tests were conducted at 800°C by feeding humidified fuel to the anode and air (150 mL/min) to the cathode. In this cell test configuration, it is difficult to increase the fuel utilization because an excess amount of gas flow is needed. Therefore, high fuel utilization conditions were simulated by adjusting the anode gas composition to that typically found downstream of the SOFC stack. Fuel utilization of 80% was simulated by using a mixture of H_2 (20 mL/min), H_2O (80 mL/min), and N_2 (100 mL/min), herein referred to as “simulated Uf = 80%”. Fuel utilization of 95% was simulated by using a mixture of H_2 (5 mL/min), H_2O (95 mL/min), and N_2 (100 mL/min), herein referred to as “simulated Uf = 95%”. The concentration of water vapor was controlled by the temperature of the humidifier. N_2 gas was mixed in

as an inert carrier gas to avoid liquid water condensation in the anode gas piping, and to stabilize the cell performance under such a high water vapor concentration. Because the pO_2 in the anode is predominantly determined by the H_2:H_2O ratio, the influence of the N_2 inclusion is considered to be small.

The cell voltage was kept constant at 0.6 V or 0.5 V by regulating the current, and changes in the performance over time were measured up to 1000 h. Automatic SOFC test systems (Toyo Corporation) were used for the gas supply and electrochemical measurements. During operation, the current interrupt method was applied simultaneously and continuously. In this method, the change in voltage within 20 μs after current interruption was measured to evaluate the ohmic loss. The remaining voltage losses, including activation overpotential and concentration overpotential, were labelled as polarization.

Cathode potential and anode potential were evaluated versus the reference electrode. When no current is applied (i.e. open circuit conditions), the cathode potential and the anode potential are determined only by the gas composition. The cathode potential under open circuit conditions is almost zero, because the reference electrode is exposed to the same atmosphere as the cathode. The anode potential under open circuit conditions is determined by the fuel gas composition. When the current load increases, the cathode potential decreases and the anode potential increases due to the polarization induced by each electrode reaction and the ohmic losses in the electrolyte. The ohmic losses in the electrolyte can be divided into anode-side and cathode-side losses using the reference electrode. Because the electrolyte plate is relatively thick (0.2 mm), and the reference electrode is located far enough away from the cathode compared to the electrolyte thickness, the potential within the electrolyte can be detected on the condition that oxygen ions flow perpendicularly to the electrolyte plate [18-19]. Because ohmic losses in the electrolyte do not affect Ni oxidation in the anode, they are excluded from the anode potential when we discuss Ni oxidation. At the beginning of this study, it was not clear whether ohmic losses in the anode would affect Ni oxidation or not. Therefore, two types of “compensated anode potentials” were calculated for discussing the cause of Ni oxidation. The first, E_{CT} was compensated by the ohmic losses coming from both the electrolyte and the anode, and E_{CT} is considered to reflect the localized oxygen partial pressure pO_2 at the electrode reaction site. The second, E_{CE} was compensated by the ohmic losses coming only from the electrolyte. As described below, it was confirmed that ohmic losses in the anode

were negligible in the initial stages of operation. Because ohmic loss in the electrolyte are considered to be constant, E_{CE} was calculated using the initial ohmic losses.

The microstructure of the anode before and after the durability tests was observed using a focused ion beam scanning electron microscope (FIB-SEM; FEI Helios NanoLab 600i). Cross-sectional backscattered electron images were obtained to distinguish Ni and Zr (in ScSZ) by their difference in contrast.

Results and discussion

Figure 4 shows the performance of a cell operating at 0.6 V for 100 h under the simulated Uf = 80% condition. The current density increased from 0.65 to 0.74 Acm^{-2} during operation. This enhancement in current density is due to a decrease in cathode polarization, as described below. Because the cell voltage was kept at a constant value, both the cathode potential and anode potential measured by the reference electrode changed similarly over time, increasing by 8 mV. Figure 5 shows the cathode performance and anode performance measured by varying the current density before (0 h), and after 100 h cell operation. As shown in Fig. 5 (a), the cathode polarization decreased after 100 h of operation, although the cathode-side ohmic losses did not change. The sum of the cathode-side and anode-side ohmic losses at 0 h was almost equal to the value calculated from the resistance of the ScSZ electrolyte (0.2 Ω cm^2 at 800°C). This result indicates that ohmic losses in the anode are negligible in the initial stages of cell operation.

Figure 6 shows the cell performance during operation at 0.6 V for 1000 h under the simulated Uf = 80% condition. The two different types of compensated anode potentials, E_{CT} and E_{CE} are shown in Fig. 6 (b), and compared with the Ni oxidation potential (−0.701 V) and the potential under open circuit conditions (−0.862 V). The difference between E_{CT} and the open circuit potential corresponds to the anode polarization. The initial anode polarization was 10 mV and increased by 36 mV during 1000 h of operation, which indicates an increase in the chemical potential of oxygen at the electrode reaction site due to degradation. E_{CE} increased by 68 mV during 1000 h of operation. The difference in E_{CE} and E_{CT} corresponds to ohmic losses in the anode, and these increased from a negligible amount to 32 mV over 1000 h of operation. This result suggests that the cell degradation was accompanied a disruption of the connectivity of the Ni network. Under these operating conditions, although E_{CT} and E_{CE} in-

creased with time, they were still lower than the Ni oxidation potential by more than 80 mV after 1000 h. Because the cell voltage was kept constant, the current density gradually decreased over time in the latter half of the 1000 h operation due to anode degradation. The cathode potential increased until the end of the test because of the decrease in current density.

Figure 7 shows the cell performance during operation at 0.5 V under the simulated Uf = 80% condition. The current density and anode potential were higher than in the case of Fig. 6 due to the lower operating cell voltage. The initial ohmic resistance was 0.130 Ω cm^2 for the cathode side and 0.055 Ω cm^2 for the anode side. The sum of the ohmic losses is slightly lower than the resistance of the ScSZ electrolyte, which suggests the possibility of a slight increase in local temperature caused by the higher current density. Under these operating conditions, significant performance degradation occurred after 80 h. The current density and E_{CE} started to fluctuate after 15 h, and this fluctuation became much more significant after 80 h. Figure 8 shows the change in cathode and anode potentials during the performance fluctuation from 30 to 40 h, and from 85 to 90 h. The potential−current density curves measured after 100 h of operation are also plotted in the figure. The performance fluctuation after 80 h is attributed to the change in anode performance, because the anode potential varied inversely with current density while the cathode potential varied proportionally with the change in current density. Because the cell voltage was kept constant, the drastic change and fluctuation in anode performance was compensated for by changing the current density. The initial anode polarization was 56 mV and it increased by 10 mV during the initial 80 h operation period. This result suggests that the localized chemical potential of oxygen at the electrode reaction site did not increase very much before significant degradation occurred at 80 h. E_{CE} increased by 40 mV during the initial 80 h of operation, which means that ohmic loss in the anode increased from a negligible level to around 30 mV. However, E_{CT} and E_{CE} were still lower than the Ni oxidation potential by more than 60 mV shortly before the significant fluctuation occurred.

Next, the performance fluctuation was analyzed in detail. Figure 9 (a) shows the change in current density over time from 30 to 40 h. The current density fluctuated from 1.02 A cm^{-2} to 1.07 A cm^{-2}. As shown in Fig. 9 (b), E_{CE} increased when the current density decreased. The response is contrary to that in normal cases, in which the anode potential should decrease when the current density decreases. The dotted diagonal lines in Figs. 9 (b) and (c) were drawn from the average values during operation to the values under open circuit conditions, and indicate the trend that these characteristic values normally follow due to the change in

current density. In contrast, E_{CT} did not change significantly, suggesting little change in the chemical potential of oxygen at the electrode reaction sites. From Figs. 9 (c) and (d), the fluctuation of the ohmic resistance was found to be the main cause of the phenomena, which led to the increase in ohmic losses, a decrease in current density, and vice versa. The fluctuation of ohmic resistance occurred at a slow pace, roughly once or twice per hour. The magnitude of the slow fluctuation of ohmic losses was about 20 mV. It can be seen in Fig. 9 (a) that a much faster fluctuation also occurred, faster than the data acquisition interval (10 s). The magnitude of this fast fluctuation was about 5 mV and could not be attributed to ohmic loss or polarization.

Figure 10 (a) shows the change in current density over time from 85 to 90 h. The current density dropped drastically from 1.1 A cm^{-2} to between 0.2 and 0.5 A cm^{-2} and recovered repeatedly. The change in ohmic resistance was significant, as shown in Fig. 10 (d), and was the main cause of the performance fluctuations. When the current density started to decrease from 1.1 A cm^{-2}, E_{CE} increased drastically, while E_{CT} did not change, as shown in Fig. 10 (b). The two types of compensated anode potentials behaved as follows:

1) First, E_{CE} increased because ohmic losses in the anode increased.
2) Then, E_{CE} reached the Ni oxidation potential of −0.701 V.
3) Then, E_{CT} increased dramatically, eventually reaching the Ni oxidation potential.
4) Finally, both potentials returned to their original values.

The above sequence indicates that E_{CE} is the trigger that causes Ni oxidation in the anode. Therefore, ohmic losses in the anode affect Ni oxidation. E_{CT} then increases as a result of Ni oxidation, reflecting the increase in the localized chemical potential of oxygen at the electrode reaction sites.

Figure 11 shows the cell performance during operation at 0.6 V under the simulated Uf = 95% condition. The initial ohmic resistance was 0.155 Ω cm^2 for the cathode side and 0.053 Ω cm^2 for the anode side. The sum of the ohmic losses was almost equal to the resistance of the ScSZ electrolyte, which means negligible ohmic losses occurred in the electrodes. E_{CE} and E_{CT} are also shown in Fig. 11 (b) compared with the Ni oxidation potential (−0.701 V) and the open circuit potential (−0.794 V). Under these operating conditions, significant performance degradation occurred after 800 h. The initial anode polarization was 37 mV and it increased by 20 mV during the first 800 h of operation. E_{CT} was −0.737 V at 800 h, which was still lower than the Ni oxidation potential. This result suggests that the localized chemical potential of

oxygen at the electrode reaction site did not reach conditions required for Ni oxidation. On the other hand, E_{CE} increased by 56 mV during the first 800 h of operation, which is a 36 mV larger increase compared with E_{CT}, due to the increase in ohmic losses in the anode. Therefore, the potential required for Ni oxidation was reached. In comparison with the case of operation at 0.5 V under the simulated Uf = 80% condition (Fig. 7), these compensated anode potentials were closer to the Ni oxidation potential from the beginning of the operation. However, it took much more time before significant degradation occurred. Significant degradation occurred when E_{CE} came close to the Ni oxidation potential, which suggests that it was induced by Ni oxidation.

Figure 12 (a) shows the change in current density over time from 50 to 60 h. The current density abruptly dropped and recovered periodically by more than 0.1 A/cm^2, roughly once every three hours. The circled data in Figs. 12 (b), (c), and (d) were affected by this change. This phenomenon was probably caused by temporary blocking of the gas piping due to water condensation in the fuel supply and exhaust system, the anode polarization was directly affected, as shown in Fig. 12 (c). Anode polarization measured in this study includes all non-ohmic losses such as activation overpotential and concentration overpotential, and also voltage changes such as by a change in the gas pressure. If this drastic but temporary change is neglected, the current density fluctuated between 0.3 and 0.35 A cm^{-2}. The fluctuation was caused by the change in anode polarization, which increased when the current density decreased. This response is the opposite trend to that during normal operation, in which anode polarization should decrease when the current density decreases. The dotted diagonal lines in Figs. 12 (b) and (c) are drawn from the average values during operation to the values under open circuit conditions, and indicate the trend that these characteristic values normally follow due to the change in current density. In this case, the ohmic resistance shown in Fig. 12 (d) seems to be independent of the fluctuation. The fluctuation occurred faster than the data acquisition interval (10 s), with an anode polarization amplitude of about 20 mV. In general, anode polarization is considered to be dominated either by dissociative adsorption of reactants or surface diffusion of the adsorbed species on the Ni surface [20,21]. Bessler et al. [21] reported that polarization losses at high overpotential are due to blocking of the Ni surface with OH. Fluctuation of the current density was observed under weakly humidified methane fuel [23] and under sulfur-containing hydrogen [24], and these phenomena are considered to have been affected by Ni surface reactions. These kinds of overpotential are included. However, the fluctuation observed in this study might have been dominated by a fluctuation of gas pres-

sure due to water condensation in the fuel supply and exhaust system, although this is not yet clear. Similar fluctuation phenomena of the current density under highly humidified conditions were also reported in Refs. 2 and 17, even though the reason has not been clarified. This kind of fluctuation should be carefully prevented to avoid unexpected degradation.

Figure 13 shows the change in current density over time from 900 to 950 h after cell operation at 0.6 V under the simulated Uf = 95% condition. Fast fluctuations with smaller characteristic amplitude (<0.05 A cm^{-2}) and slow fluctuations with a larger characteristic amplitude (<0.15 A cm^{-2}) can be distinguished. Figure 14 (a) shows the data for 908 to 910 h. The fluctuation was analyzed by dividing the duration into two time periods: Period I (from 908.0 to 909.0 h) and Period II (from 909.2 to 910.0 h), corresponding to the slow fluctuations. In Period I, E_{CE} significantly exceeded the Ni oxidation potential (−0.701 V), as shown in Fig. 14 (b). Although anode polarization fluctuated significantly, as shown in Fig. 14 (c), the amplitude was roughly 20 mV, almost the same as that before degradation (Fig. 12 (c)). The ohmic resistance fluctuated after degradation, as shown in Fig. 14 (d). In Period II, the current density was higher than that in Period I. E_{CE} remained in the region around the Ni oxidation potential. The anode polarization and ohmic resistance decreased compared with Period I. The behavior of E_{CE} crossing the Ni oxidation potential back and forth suggests that Ni oxidation (Period I) and reduction (Period II) occurred repeatedly. It is therefore concluded that volume expansion by Ni oxidation temporarily recovered the Ni(NiO) network and decreased E_{CE}, leading to this observed performance fluctuation.

The effect of ohmic loss on Ni oxidation is discussed as follows. It has been reported that the active thickness of an Ni/YSZ cermet anode is approx. 10 μm from the electrolyte/anode interface, which is limited by the ionic resistance of the electrolyte phase (YSZ) in the anode [25,26]. In impedance measurements, the ionic resistance appears under high-frequency regions [27] and the voltage loss caused by ionic resistance is incorporated into ohmic losses in the present study. Ohmic losses in the anode may arise from disruption of the interconnected Ni network, which is necessary for the electrons to flow smoothly from the electrode reaction sites to the current collector. As shown in Fig. 15, disconnection of the Ni network will isolate some electrode reaction sites and make them unavailable. Then, electrode reactions must occur further away from the electrolyte/anode interface. Oxygen ions will flow further into the anode and cause an increase in ohmic losses. As a result, isolated Ni near the electrolyte will be exposed to greater oxidizing conditions due to the increase in ohmic losses. When Ni oxi-

dation becomes more severe, the volumetric changes may cause mechanical damage [9,11-13,29-30] even in the ScSZ network. The performance fluctuations shown in Fig. 10 or Fig. 14, however, show that such interruption of the ScSZ network did not occur in this case, because the ohmic resistance repeatedly returned to the original value.

For the two operating conditions, 0.5 V under the simulated Uf = 80% condition (Fig. 10), and 0.6 V under the simulated Uf = 95% condition (Fig. 14), similar performance fluctuation related to Ni oxidation occurred, in which E_{CE} moved back and forth crossing the Ni oxidation potential at a slow pace, roughly once per hour. This fluctuation probably reflects the following sequential events: i) interruption of the Ni network; ii) an increase in E_{CE}, iii) Ni oxidation and associated volume expansion; iv) recovery of the Ni(NiO) connection; v) a decrease in E_{CE}, and vi) Ni reduction. Changes in morphology and volume expansion of Ni particles due to oxidation have been previously reported in many studies [9,14,29-33]. The performance fluctuations observed in the early stage of operation, shown in Fig. 9, must also be associated with the above-mentioned phenomena, although the reason is not yet clear. Oxidation and reduction on the Ni surface occurring in the process of electrode reaction may be behind this observation.

The reason for the disruption of the connectivity of the Ni network is the agglomeration of Ni particles in the anode. By comparing the two operating conditions, E_{CE} at 0.6 V under the simulated Uf = 95% condition was closer to the Ni oxidation potential from the beginning. However, it took more time (~800 h) before oxidation-induced degradation occurred, compared to that at 0.5 V under the simulated Uf = 80% condition (~80 h). In the case of operation at 0.5 V under the simulated Uf = 80% condition, the high current density accompanied by large polarization might have promoted Ni agglomeration, and accelerated disruption of the Ni network. For the mechanism of Ni agglomeration, an increase in the localized pH_2O at the electrode reaction sites [6,22] or localized oxidation of Ni which enhances cation diffusion [5] are possible causes.

Figure 16 shows cross-sectional backscattered electron images for (a) the initial anode, and (b) the anode after a 1000 h durability test at 0.6 V under the simulated Uf = 95% conditions. The distribution of Ni particles in the initial anode appears to be somewhat sparse near the electrolyte, in which lack of connectivity of the Ni network may be expected when Ni particles begin to agglomerate during cell operation. The fluctuation of ohmic resistance observed

in Figs. 9 and 10 might have come from this poor Ni network, and the drastic increase in ohmic resistance after 80 h originated from the insufficient connectivity of Ni, coupled with the higher current density. Significant change in the microstructure could not be distinguished for the anode after the durability test. It was difficult to explain the cell performance degradation by microstructural analysis, because the anode presumably experienced repeated oxidation-reduction cycles, and the ex-situ SEM image does not necessarily represent the situation during operation. It is also not easy to distinguish the extent of, or changes in Ni connectivity using this technique.

The above-mentioned results firstly suggest the importance of Ni connectivity, as already recognized by preceding studies [3,28,30,33,36]. Otherwise, degradation can be abruptly induced by the agglomeration of Ni, especially under high current density conditions. Ni oxidation can be caused not only by an increase in polarization, but also by ohmic losses in the anode. Therefore, ohmic losses in the anode should be included in the "anode overpotential" in the theoretical calculations shown in Fig. 2. To evaluate the durability of the Ni anode, the compensated anode potential E_{CE}, which includes ohmic losses in the anode, is useful for forecasting Ni oxidation. To improve the durability under high fuel utilization, it is essential to modify the microstructure to suppress Ni agglomeration, which tends to be promoted under high $p\mathrm{H_2O}$ conditions [2-7]. Stable operation is possible under the operating conditions in which E_{CE} does not come close to the Ni oxidation potential, assuming a stable Ni network. When the operating conditions exceeds this limitation, a continuous reduction-oxidation may occur in the anode. The volumetric changes during these conversions firstly cause the performance fluctuation as mentioned above, and may also cause mechanical damage like disruption of the Ni network (or even the ScSZ network), leading to a significant increase in the anode overpotential. In a real SOFC stack, gas distribution related to the cell and stack structure should be carefully considered. However, limitation of the gas distribution directly affects the anode potential. Therefore, discussion of the durability of the Ni anode is also highly applicable to SOFC stacks.

Conclusions

During operation at 0.5 V under simulated Uf = 80% conditions, the ohmic resistance fluctuated slightly from the early stages of operation, and became much more significant after 80

h. This degradation appears to have originated from the insufficient connectivity of Ni, due to the high current density and large polarization, promoting Ni agglomeration. The significant fluctuation after 80 h resulted from the repeated oxidation and reduction of Ni. The compensated anode potential that includes ohmic losses in the anode (E_{CE}), was the trigger that caused Ni oxidation. Ohmic losses in the anode are considered to affect Ni oxidation by exposing Ni near the electrolyte to an oxidizing atmosphere with the increase in oxygen ion flow. During operation at 0.6 V under the simulated Uf = 95% conditions, polarization fluctuated from the early stages of operation, which may be related to the highly humidified fuel. Significant degradation occurred when E_{CE} came close to the Ni oxidation potential, which suggests that Ni oxidation induced this degradation. After degradation, fluctuation of the ohmic resistance also occurred, suggesting the repeated oxidation and reduction of Ni. To evaluate the durability of the Ni anode, the compensated anode potential E_{CE} is useful for forecasting Ni oxidation. Stable operation is possible under conditions in which E_{CE} does not come close to the Ni oxidation potential, assuming a stable Ni network.

Acknowledgments

This research was supported by the NEDO project “Technology development for SOFC commercialization promotion. Basic study on rapid evaluation method of SOFC durability.” The initial stage of this study was partly supported by the Center of Innovation Program of the Japan Science and Technology Agency (JST).

References

1. Fang Q, Blum L, Peters R, Peksen M, Batfalsky P, Stolten D. SOFC stack performance under high fuel utilization. Int J Hydrogen Energy 2015;40:1128–1136. https://doi.org/10.1016/j.ijhydene.2014.11.094.
2. Holzer L, Iwanschitz B, Hocker Th, Munch B, Prestat M, Wiedenmann D, Vogt U, Holtappels P, Sfeir J, Mai A, Graule Th. Microstructure degradation of cermet anodes for solid oxide fuel cells: Quantification of nickel grain growth in dry and in humid atmospheres. J Power Sources 2011;196:1279–94. https://doi.org/10.1016/j.jpowsour.2010.08.017.
3. Matsui T, Kishida R, Kim JY, Muroyama H, Eguchi K. Performance Deterioration of Ni-YSZ Anode Induced by Electrochemically Generated Steam in Solid Oxide Fuel Cells. J Electrochem Soc 2010;157:B776–81. doi:10.1149/1.3336830.

4. Matsui T, Kishida R, Muroyama H, Eguchi K. Comparative Study on Performance Stability of Ni-Oxide Cermet Anodes under Humidified Atmospheres in Solid Oxide Fuel Cells. J Electrochem Soc 2012;159:F456–60. doi:10.1149/2.053208jes.
5. Lee YH, Muroyama Matsui T, Eguchi K. Degradation of nickel–yttria-stabilized zirconia anode in solid oxide fuel cells under changing temperature and humidity conditions. J Power Sources 2014;262:451–6. https://doi.org/10.1016/j.jpowsour.2014.03.031.
6. Sehested J, Gelten JAP, Remediakis IN, Bengaard H, Nørskov JK. Sintering of nickel steam-reforming catalysts: effects of temperature and steam and hydrogen pressures. J Catal 2004;223:432–43. https://doi.org/10.1016/j.jcat.2004.01.026.
7. Hagen A, Barfod R, Hendriksen PV, Liu YL, Ramousse S. Degradation of Anode Supported SOFCs as a Function of Temperature and Current Load. J Electrochem Soc 2006;153:A1165–71. doi:10.1149/1.2193400.
8. Hanasaki M, Uryu C, Daio T, Kawabata T, Tachikawa Y, Lyth SM, Shiratori Y, Taniguchi S, Sasaki K. SOFC Durability against Standby and Shutdown Cycling. J Electrochem Soc 2014;161:F850–60. doi:10.1149/2.0421409jes.
9. Sumi H, Kishida R, Kim JY, Muroyama H, Matsui T, Eguchi K. Correlation Between Microstructural and Electrochemical Characteristics during Redox Cycles for Ni–YSZ Anode of SOFCs. J Electrochem Soc 2010;157:B1747–52. doi:10.1149/1.3491345.
10. Iwanschitz B, Sfeir J, Mai A, Schutze M. Degradation of SOFC Anodes upon Redox Cycling: A Comparison Between Ni/YSZ and Ni/CGO. J Electrochem Soc 2010;157:B269–78. doi:10.1149/1.3271101.
11. Heo YH, Lee JW, Lee SB, Lim TH, Park SJ, Song RH, Park CO, Shin DR. Redox-induced performance degradation of anode-supported tubular solid oxide fuel cells. Int J Hydrogen Energy 2011;36:797-804. https://doi.org/10.1016/j.ijhydene.2010.10.038.
12. Monzon H, Laguna-Bercero MA. Redox-cycling studies of anode-supported microtubular solid oxide fuel cells. Int J Hydrogen Energy 2012;37:7262-7270. https://doi.org/10.1016/j.ijhydene.2011.10.026.
13. Kim YJ, Lee MC. Evaluation of the thermal and structural stability of planar anode-supported solid oxide fuel cells using a 10 × 10 cm^2 single-cell test. Int J Hydrogen Energy in Press. https://doi.org/10.1016/j.ijhydene.2018.08.099.
14. Hatae T, Matsuzaki Y, Yamashita S, Yamazaki Y. Current density dependence of changes in the microstructure of SOFC anodes during electrochemical oxidation. Solid State Ionics 2009;180:1305–10. https://doi.org/10.1016/j.ssi.2009.08.003.

15. Chen G, Guan G, Abliz S, Kasai Y, Abudula A. Rapid degradation mechanism of Ni-CGO anode in low concentrations of H_2 at a high current density. Int J Hydrogen Energy 2011;36:8461–67. https://doi.org/10.1016/j.ijhydene.2011.04.046.
16. Brus G, Miyoshi K, Iwai H, Saito M, Yoshida H. Change of an anode's microstructure morphology during the fuel starvation of an anode-supported solid oxide fuel cell. Int J Hydrogen Energy 2015;40:6927-6934. https://doi.org/10.1016/j.ijhydene.2015.03.143.
17. Mizusaki J, Amano K, Yamauchi S, Fueki K. Electrode reaction at Pt, O2(g)/stabilized zirconia interfaces. Part I: Theoretical consideration of reaction model. Solid State Ionics 1987;22:313–22. https://doi.org/10.1016/0167-2738(87)90149-4.
18. Winkler J, Hendriksen PV, Bonanos N, Mogensen M. Geometric Requirements of Solid Electrolyte Cells with a Reference Electrode. J Electrochem Soc 1998;145:1184-92. doi:10.1149/1.1838436.
19. Adler SB. Reference Electrode Placement in Thin Solid Electrolytes. J Electrochem Soc 2002;149:E166–72. doi:10.1149/1.1467368.
20. Mizusaki J, Tagawa H, Saito T, Kamitani K, Yamamura T, Hirano K, Ehara S, Takagi T, Hikita T, Ippommatsu M, Nakagawa S, Hashimoto K. Preparation of Nickel Pattern Electrodes on YSZ and Their Electrochemical Properties in H_2-H_2O Atmosphere. J Electrochem Soc 1994;141:2129–34. doi:10.1149/1.2055073.
21. Bessler WG. A new computational approach for SOFC impedance from detailed electrochemical reaction–diffusion models. Solid State Ionics 2005;176:997–1011. https://doi.org/10.1016/j.ssi.2005.01.002.
22. Jiao Z, Takagi N, Shikazono N, Kasagi N. Study on local morphological changes of nickel in solid oxide fuel cell anode using porous Ni pellet electrode. J Power Sources 2011;196:1019–29. https://doi.org/10.1016/j.jpowsour.2010.08.047.
23. Sands JD, Uddin J, Needham DJ. Current Oscillations in Solid Oxide Fuel Cells under Weakly Humidified Conditions. J Electrochem Soc 2016;163:F856–62. doi:10.1149/2.0701608jes.
24. Yoshizumi T, Taniguchi S, Shiratori Y, Sasaki K. Sulfur Poisoning of SOFCs: Voltage Oscillation and Ni Oxidation. J Electrochem Soc 2012;159:F693–701. doi:10.1149/2.032211jes.
25. Brown M, Primdahl S, Mogensen M. Structure/Performance Relations for Ni/Yttria-Stabilized Zirconia Anodes for Solid Oxide Fuel Cells. J Electrochem Soc 2000;147:475–85. doi:10.1149/1.1393220.

26. Nakagawa N, Nakajima K, Sato M, Kato K. Contribution of the Internal Active Three-Phase Zone of Ni-Zirconia Cermet Anodes on the Electrode Performance of SOFCs. J Electrochem Soc 1999;146:1290–95. doi:10.1149/1.1391760.
27. Ramos T, Søgaard M, Mogensen M. Electrochemical Characterization of Ni/ScYSZ Electrodes as SOFC Anodes. J Electrochem Soc 2014;161:F434–44. doi:10.1149/2.045404jes.
28. Tanasini P, Cannarozzo M, Costamagna P, Faes A, Van Herle J, Hessler-Wyser A, Comninellis C. Experimental and Theoretical Investigation of Degradation Mechanisms by Particle Coarsening in SOFC Electrodes. Fuel Cells 2009;9:740–52. https://doi.org/10.1002/fuce.200800192.
29. Hatae T, Matsuzaki Y, Yamashita S, Yamazaki Y. Destruction Modes of Anode-Supported SOFC Caused by Degrees of Electrochemical Oxidation in Redox Cycle. J Electrochem Soc 2010;157: B650–4. doi:10.1149/1.3328453.
30. Klemensø T, Chung C, Larsen PH, Mogensen M. The Mechanism Behind Redox Instability of Anodes in High-Temperature SOFCs. J Electrochem Soc 2005;152:A2186–92. doi:10.1149/1.2048228.
31. Jeangros Q, Faes A, Wagner JB, Hansen TW, Aschauer U, Van Herle J, Hessler-Wyser A, Dunin-Borkowski RE. In situ redox cycle of a nickel–YSZ fuel cell anode in an environmental transmission electron microscope. Acta Mater 2010;58:4578–89. https://doi.org/10.1016/j.actamat.2010.04.019.
32. Matsuda J, Kawasaki T, Futamura S, Kawabata T, Taniguchi S, Sasaki K. In situ transmission electron microscopic observations of redox cycling of a Ni–ScSZ cermet fuel cell anode. Microscopy 2018; 67:251–8. https://doi.org/10.1093/jmicro/dfy025.
33. Faes A, Wuillemin Z, Tanasini P, Accardo N, Van Herle J. Redox stable Ni–YSZ anode support in solid oxide fuel cell stack configuration. J Power Sources 2011;196:3553–8. https://doi.org/10.1016/j.jpowsour.2010.11.047.
34. Parikh H, Hilli H, Guire MR, Heuer AH, Liu Z, Goettler R. Long-term microstructural changes in solid oxide fuel cell anodes: 3D reconstruction. J Am Ceram Soc 2017;100:1653–60. https://doi.org/10.1111/jace.14659.
35. Zekri A, Herbrig K, Knipper M, Parisi J, Plaggenborg T. Nickel Depletion and Agglomeration in SOFC Anodes During Long-Term Operation. Fuel Cells 2017;17:359–66. https://doi.org/10.1002/fuce.201600220.
36. Jiao Z, Shikazono N, Kasagi N. Quantitative Characterization of SOFC Nickel-YSZ Anode Microstructure Degradation Based on Focused-Ion-Beam 3D-Reconstruction Technique. J Electrochem Soc 2012;159:B285–91. doi:10.1149/2.045203jes.

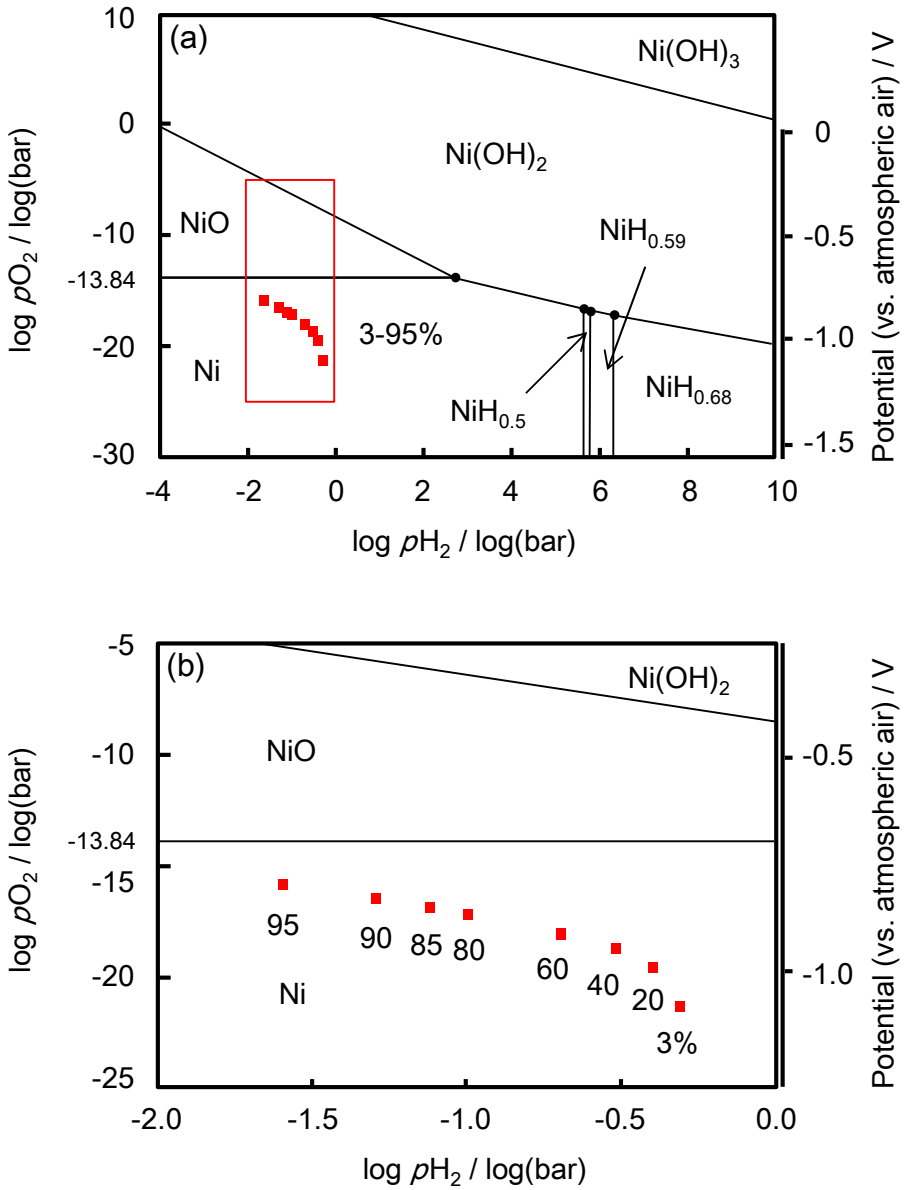

Figure 1. Phase stability diagram of the Ni-O-H system at 800°C thermochemically calculated (a) over a wide partial pressure range, and (b) in a limited partial pressure range. The H_2/O_2 partial pressure calculated under each fuel utilization (Uf) condition is also plotted in the figure.

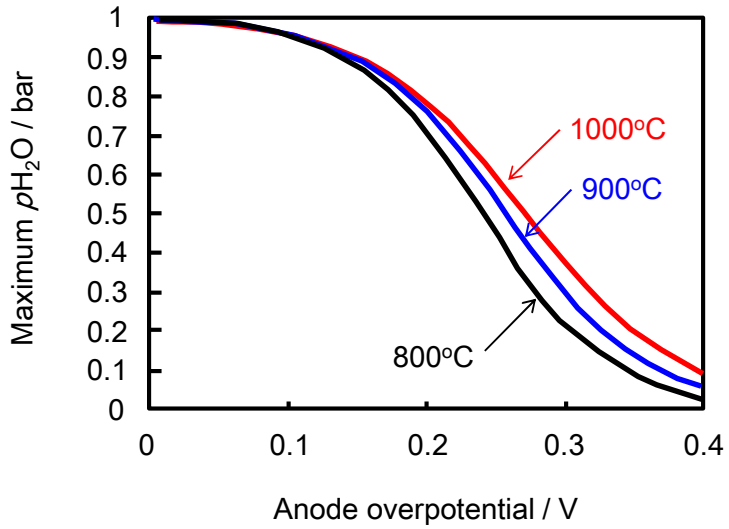

Figure 2. Maximum water vapor pressure in the H_2–H_2O system influenced by anode overpotential, in which the oxygen partial pressure will reach the Ni/NiO phase boundary at the anode reaction sites.

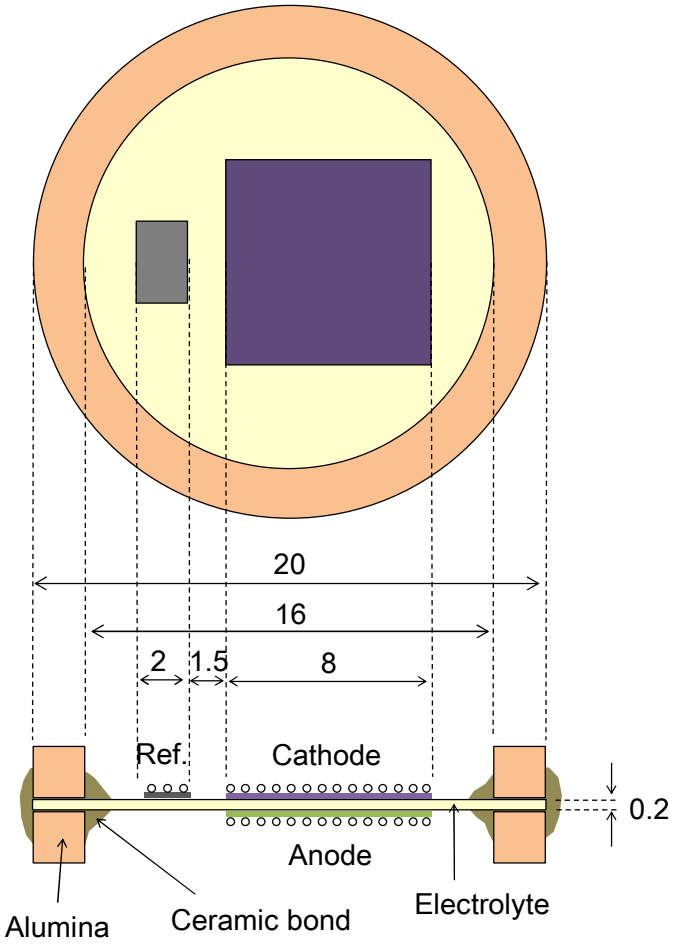

Figure 3. Configuration of the SOFC.

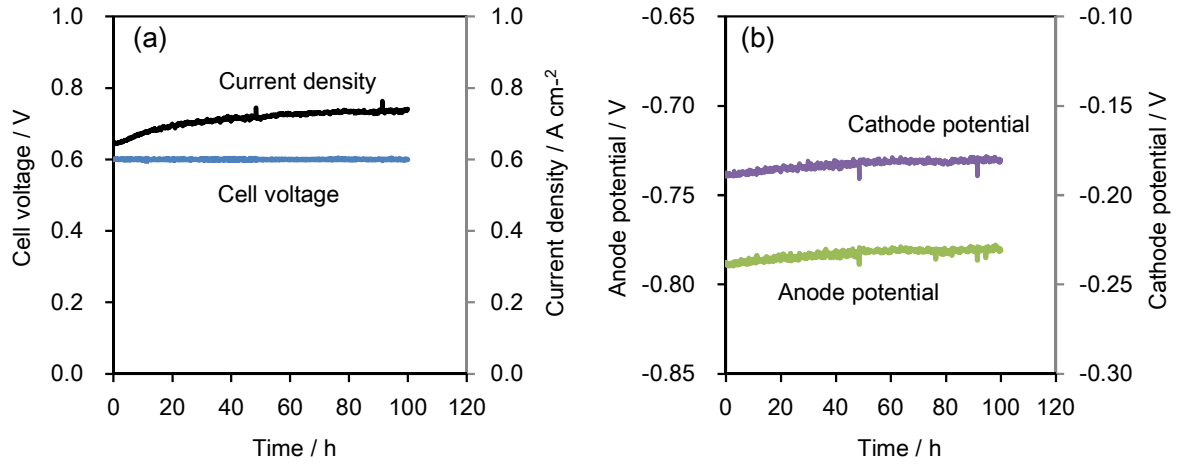

Figure 4. Performance of a cell operating at 0.6 V for 100 h under the simulated Uf = 80% condition. The temperature is 800°C; the anode gas is a mixture of H_2 (20 mL/min), H_2O (80 mL/min), and N_2 (100 mL/min). (a) Current density and cell voltage. (b) Cathode potential and anode potential measured by the reference electrode.

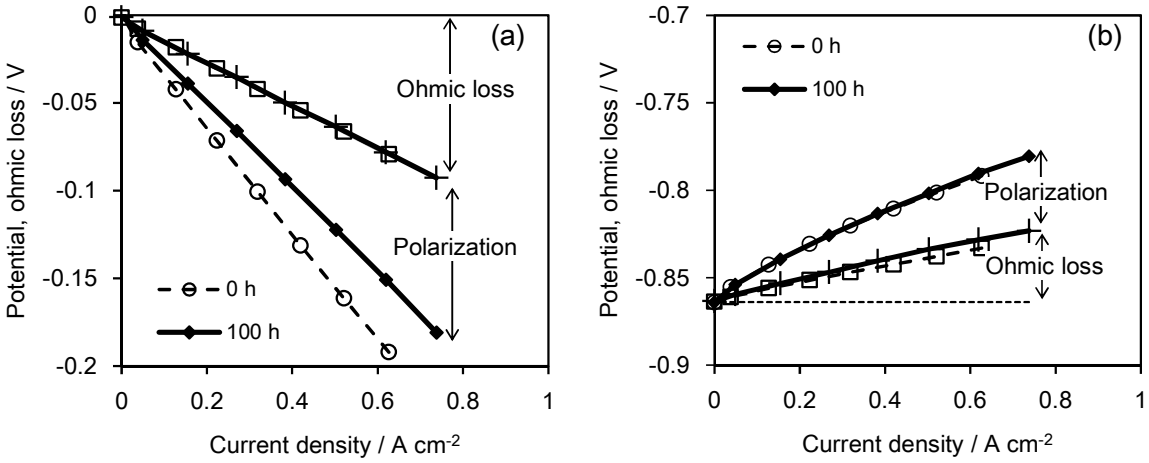

Figure 5. Cathode performance and anode performance measured by changing current density before (0 h) and after 100 h of the cell operation shown in Fig. 4. (a) Cathode potential and cathode-side ohmic losses measured by the current interruption method. (b) Anode potential and anode-side ohmic losses measured by the current interrupt method. The sum of the cathode-side and anode-side ohmic losses at 0 h was almost equal to the value calculated from the resistance of the electrolyte.

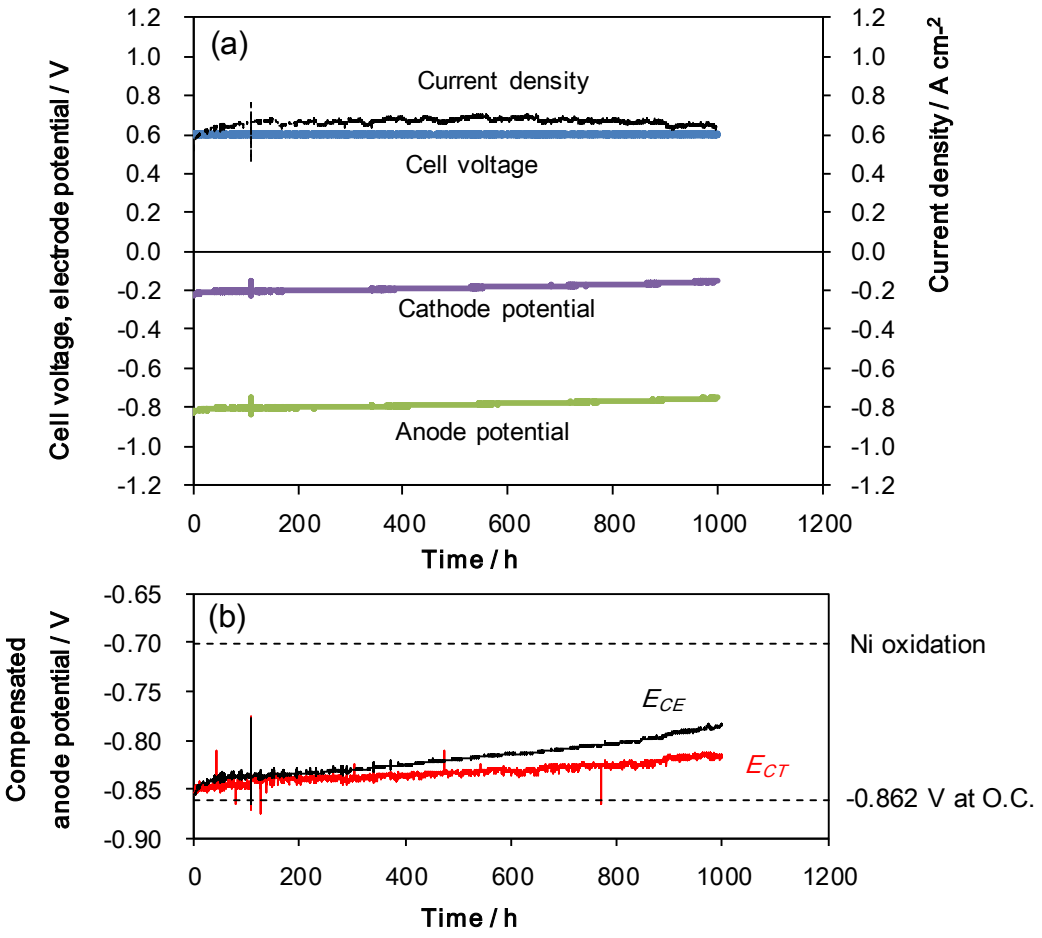

Figure 6. Performance of a cell operating at 0.6 V for 1000 h under the simulated Uf = 80% conditions. The temperature was 800°C, and the anode gas was a mixture of H_2 (20 mL/min), H_2O (80 mL/min), and N_2 (100 mL/min). (a) Current density, cell voltage, cathode potential and anode potential. (b) Two types of compensated anode potentials compared with the Ni oxidation potential (−0.701 V) and the open circuit potential (−0.862 V).

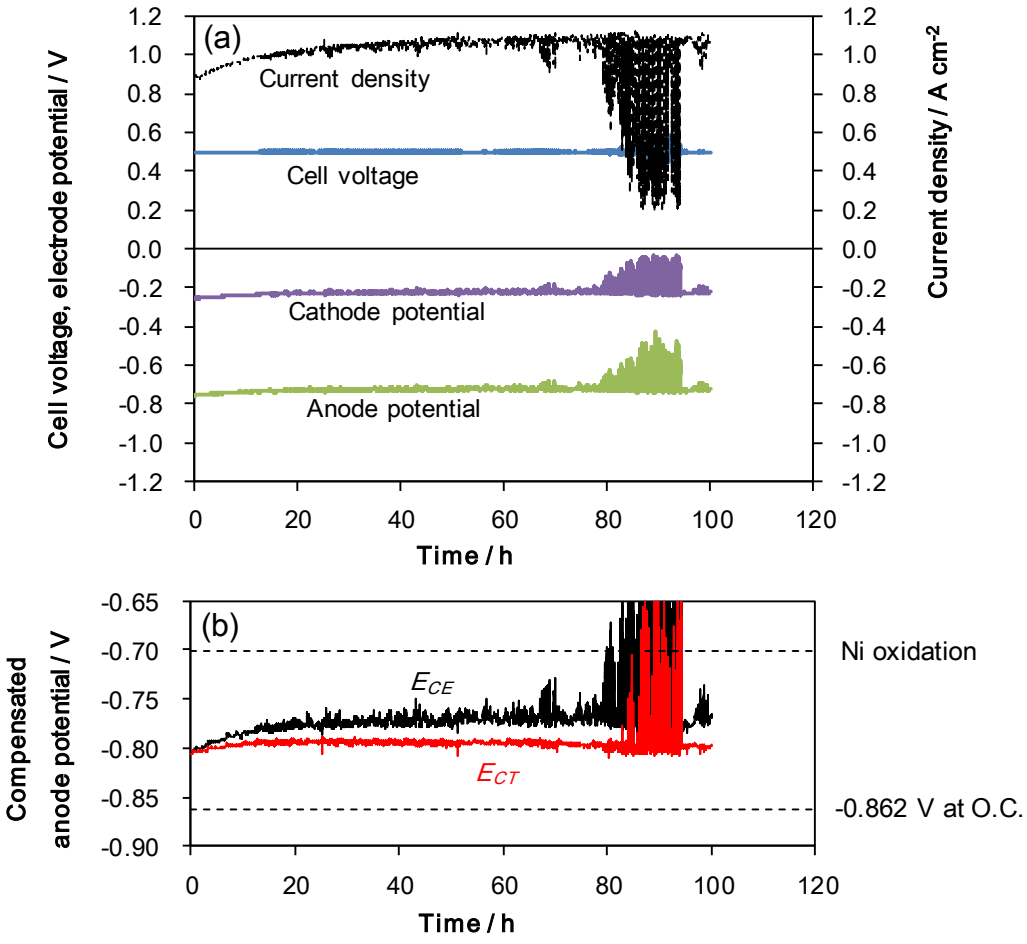

Figure 7. Performance of a cell operating at 0.5 V for 100 h under the simulated Uf = 80% conditions. The temperature was 800°C, and the anode gas was a mixture of H_2 (20 mL/min), H_2O (80 mL/min), and N_2 (100 mL/min). (a) Current density, cell voltage, cathode potential and anode potential. (b) Two types of compensated anode potentials compared with the Ni oxidation potential (−0.701 V) and the open circuit potential (−0.862 V).

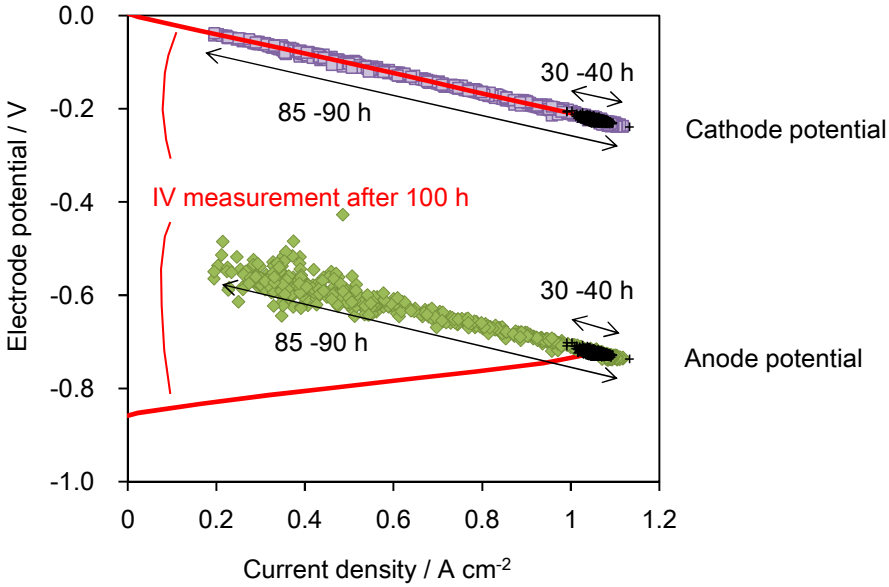

Figure 8. Change in the cathode potential and anode potential during performance fluctuation between 30 and 40 h, and between 85 and 90 h. The potential–current density curves measured after 100 h of operation are also plotted.

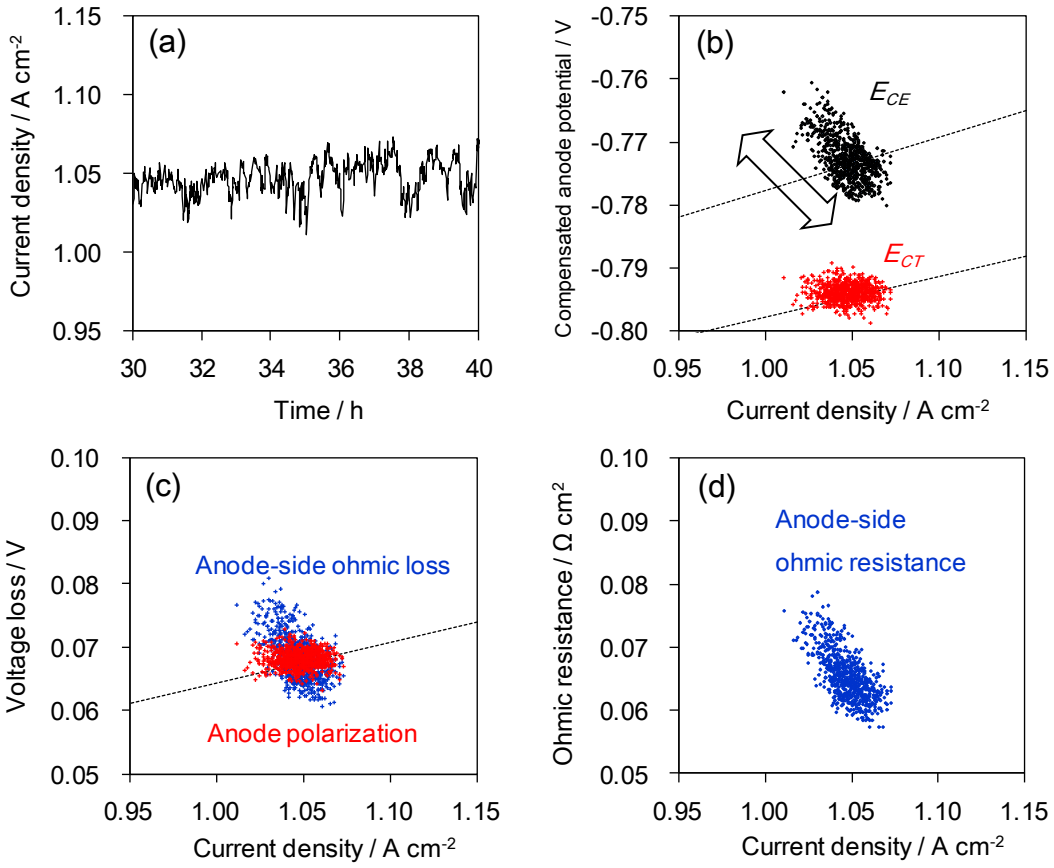

Figure 9. Fluctuation of current density and related performance changes from 30 to 40 h, before degradation in the cell test at 0.5 V under the simulated Uf = 80% conditions. (a) Change in current density over time; (b) changes in the two types of compensated anode potentials; (c) anode polarization and anode-side ohmic losses; and (d) anode-side ohmic resistance over the change in current density. The dotted diagonal lines in (b) and (c) were drawn from the average values during operation to the values under open circuit conditions, and indicate the usual trends which these characteristic values normally follow due to the change in current density.

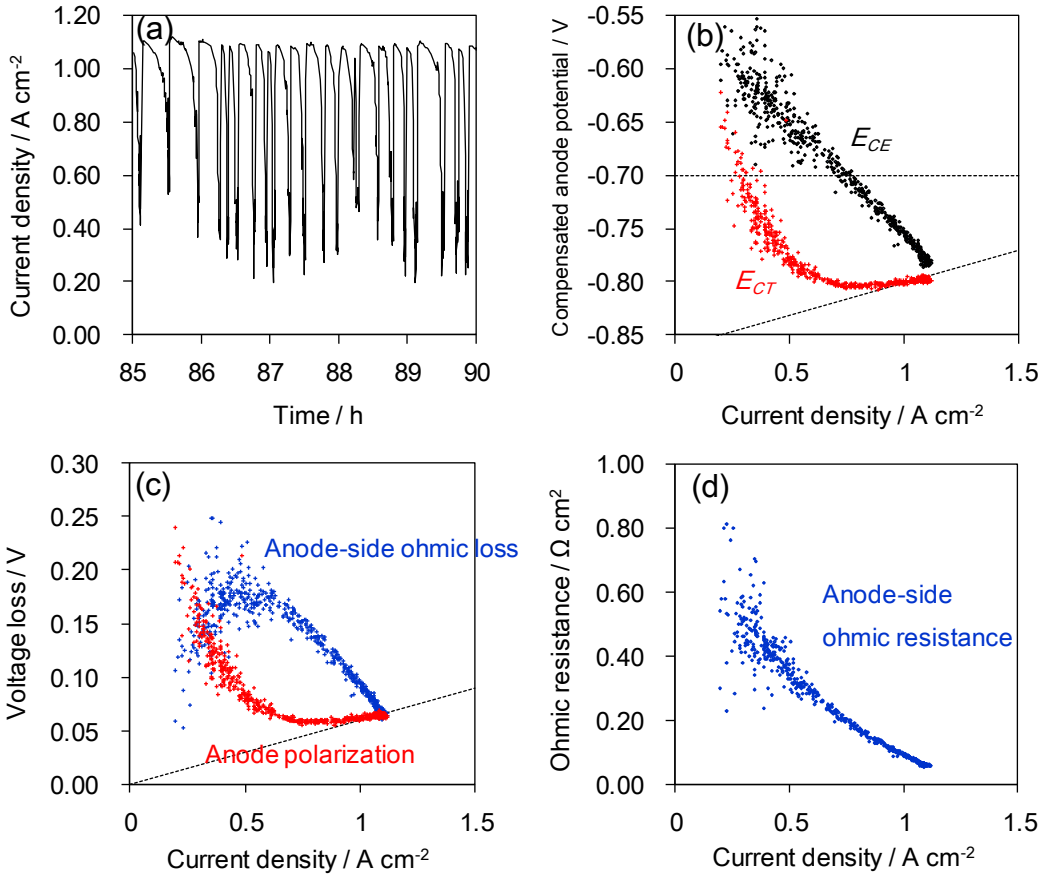

Figure 10. Fluctuation of the current density and related performance changes from between 85 and 90 h after degradation in the cell test at 0.5 V under the simulated Uf = 80% conditions. (a) Change in current density over time; (b) changes in the two types of compensated anode potentials; (c) anode polarization and anode-side ohmic losses; and (d) anode-side ohmic resistance over the change in current density. The dotted diagonal lines in (b) and (c) were drawn from the average values during operation to the values under open circuit conditions, and indicate the usual trends which these characteristic values normally follow due to the change in current density.

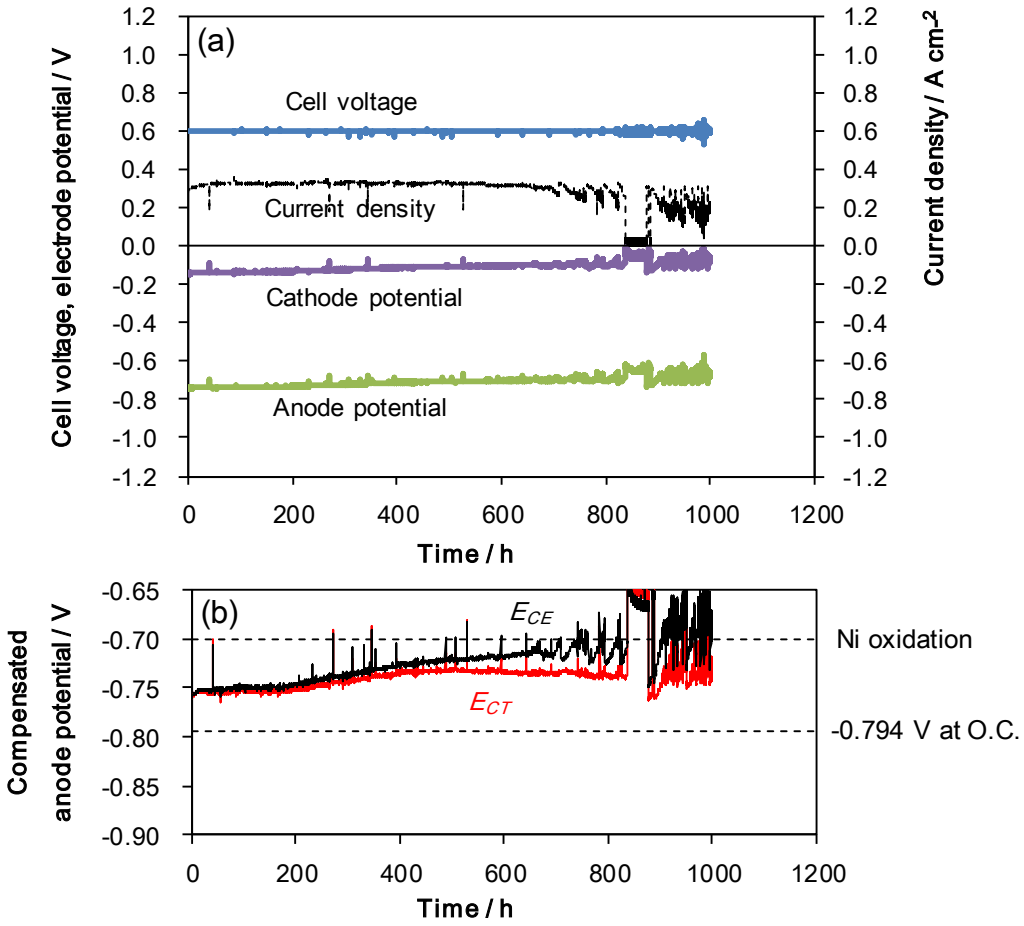

Figure 11. Performance of a cell operating at 0.6 V for 1000 h under the simulated Uf = 95% conditions. The temperature was 800°C, and the anode gas was a mixture of H_2 (5 mL/min), H_2O (95 mL/min), and N_2 (100 mL/min). (a) Current density, cell voltage, cathode potential and anode potential. (b) Two types of compensated anode potentials compared with the Ni oxidation potential (−0.701 V) and the open circuit potential (−0.794 V).

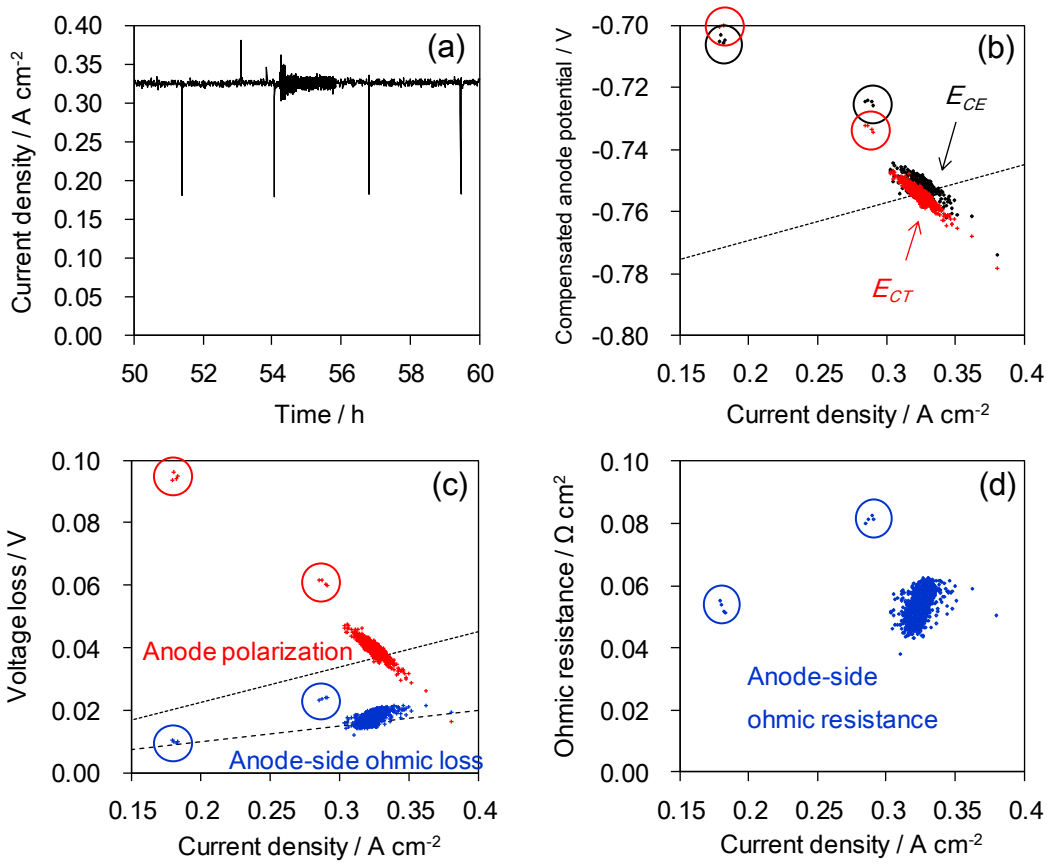

Figure 12. Fluctuation of current density and related performance changes from between 50 and 60 h, before degradation in the cell test at 0.6 V under the simulated Uf = 95% conditions. (a) Change in current density over time; (b) changes in the two types of compensated anode potentials; (c) anode polarization, anode-side ohmic loss; and (d) anode-side ohmic resistance over the change in current density. The dotted diagonal lines in (b) and (c) were drawn from the average values during operation to the values under open circuit conditions, and indicate the usual trends which these characteristic values normally follow due to the change in current density. The circled data in (b), (c), (d) were periodically obtained when the current density abruptly dropped and recovered.

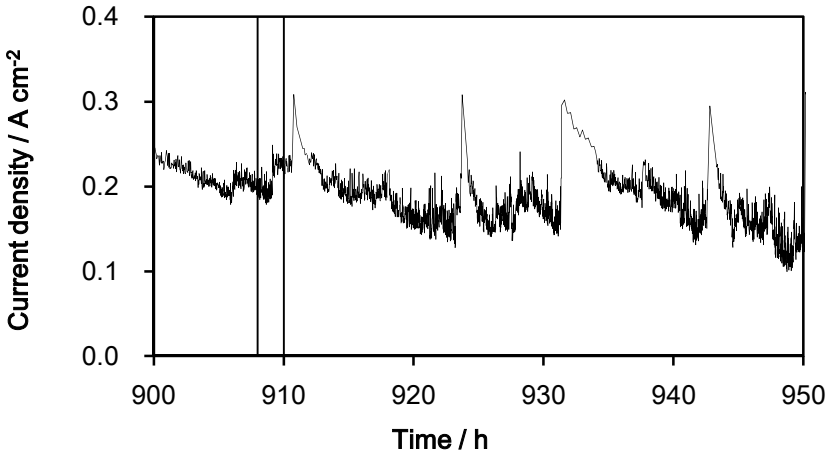

Figure 13. Change in current density over time from between 900 and 950 h, after degradation in the cell test at 0.6 V under the simulated Uf = 95% condition.

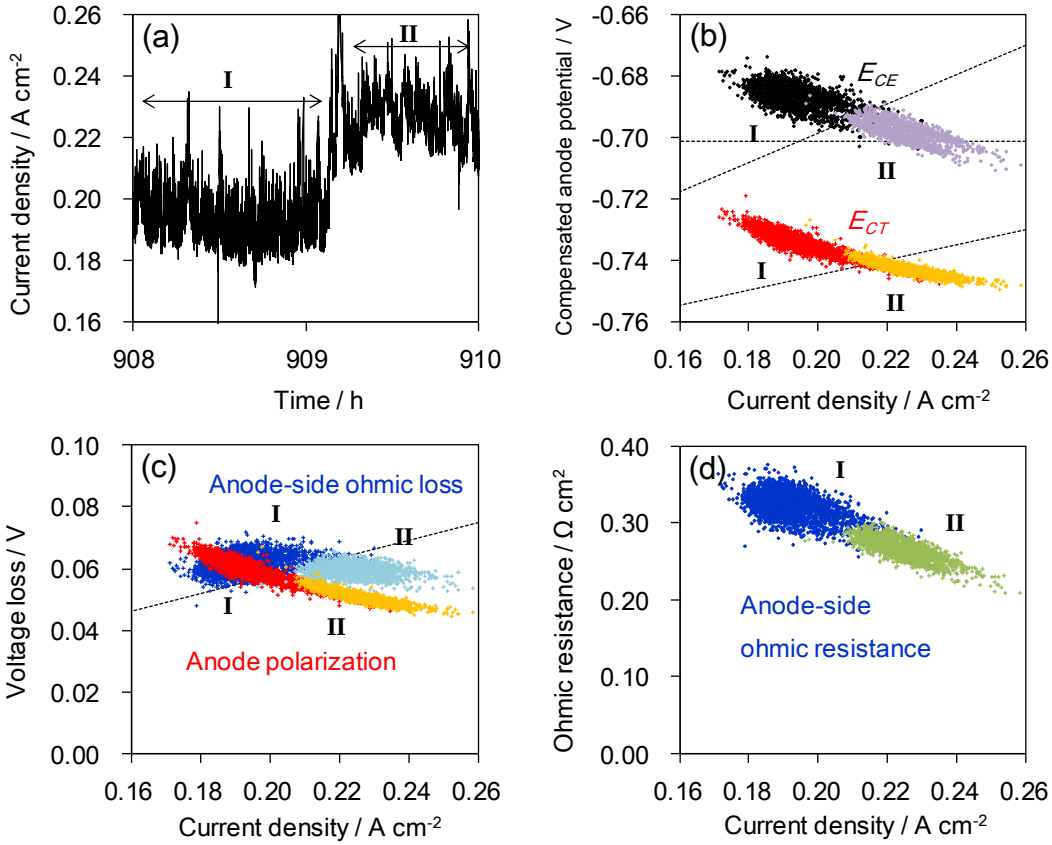

Figure 14. Fluctuation of the current density and related performance changes from between 908 and 910 h, after degradation in the cell test at 0.6 V under the simulated Uf = 95% condition. (a) Change in current density over time; (b) changes in the two types of compensated anode potentials; (c) anode polarization, anode-side ohmic loss; and (d) anode-side ohmic resistance over the change in current density. The dotted diagonal lines in (b) and (c) were drawn from the average values during operation to the values under open circuit conditions, and indicate the usual trends which these characteristic values normally follow due to the change in current density.

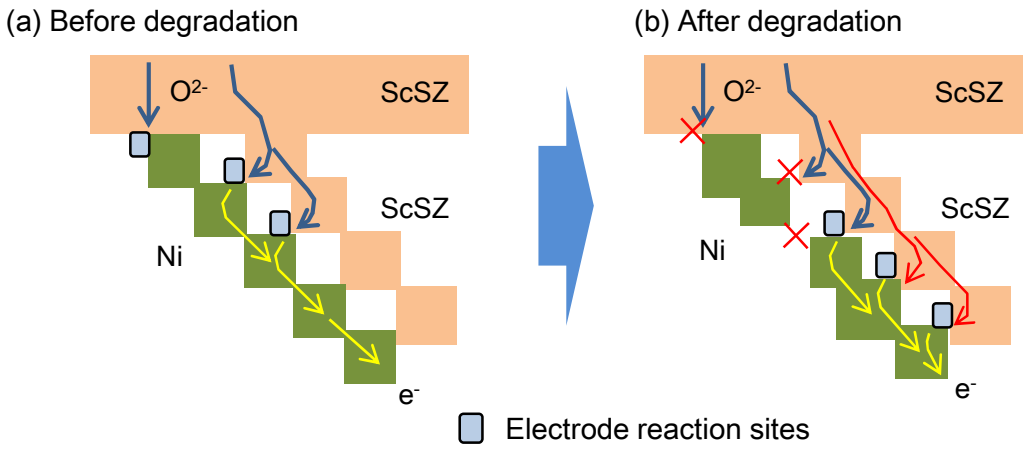

Figure 15. Schematic diagram demonstrating the effect of anode ohmic losses on Ni oxidation.

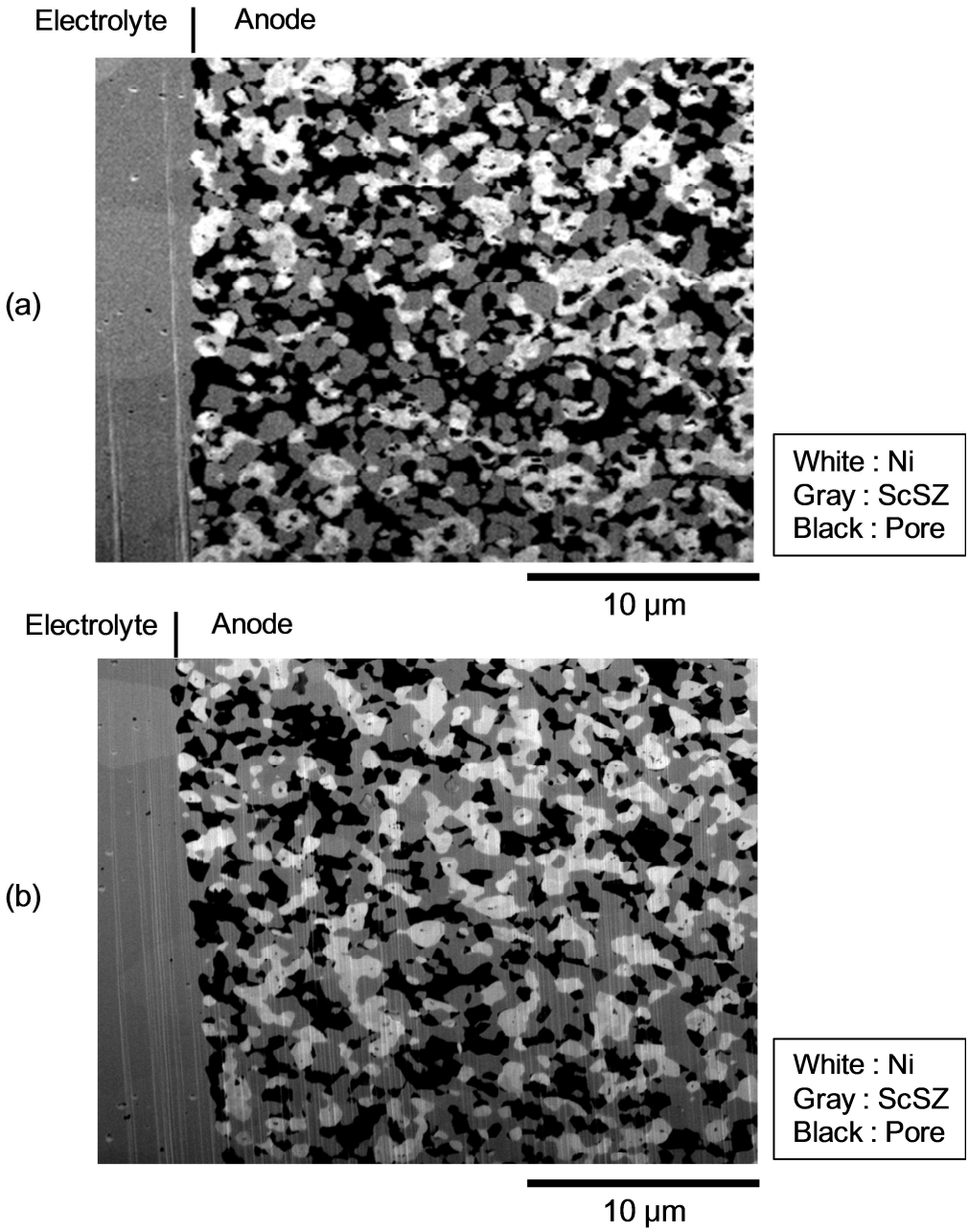

Figure 16. Cross-sectional backscattered electron images for (a) the initial anode, and (b) the anode after the 1000 h durability test at 0.6 V under the simulated Uf = 95% condition (as shown in Fig. 11).